Supporting Information

Thermal activation induced charge transfer state absorption redshift realizes strong anti-thermal quenching in Pr^{3+}-activated phosphor

Xiang Lv,[a] Ning Guo,[a,*] Song Qu,[a] Yanmei Xin,[a] Mei Yang,[b] Baiqi Shao,[c] and Ruizhuo Ouyang,[a]

[a] Department of Chemistry, University of Shanghai for Science and Technology, Shanghai 200093, P. R. China.

[b] Eye & ENT Hospital of Fudan University, Fudan University, Shanghai 200031, P. R. China.

[c] State Key Laboratory of Rare Earth Resource Utilization, Changchun Institute of Applied Chemistry, Chinese Academy of Sciences, Changchun 130022, P. R. China.

*Corresponding author: E-mail: guoning@usst.edu.cn

Author Contributions

Xiang Lv: Methodology, Validation, Formal analysis, Investigation, Data curation, Writing - original draft, Writing - review &editing. **Ning Guo**: Conceptualization, Methodology, Resources, Supervision, Funding acquisition. **Song Qu**: Methodology, Investigation. **Yanmei Xin**: Methodology, Investigation. **Mei Yang**: Methodology, Investigation. **Baiqi Shao**: Resources, Supervision, Project administration. **Ruizhuo Ouyang**: Resources, Supervision, Project administration.

1. Materials and synthesis

The $LiTaO_3$:xPr^{3+}(x = 0.000, 0.001, 0.005, 0.025) phosphors were synthesized by high temperature solid phase method. The raw materials are Li_2CO_3 (A.R), Ta_2O_5 (A.R), Pr_6O_{11} (99.99%). After weighing the raw materials strictly in accordance with the stoichiometric proportion, transferring them to agate mortar and grinding them for 30 min. The fully ground raw materials were moved to an alumina crucible with a cover and sintered at 1070 °C for 3 h in air atmosphere. After the sintered sample is cooled to room temperature, it is ground into powder and put into the sample tube for subsequent testing and characterization.

2. Effective lifetime calculation

The effective lifetime of the Pr^{3+} ions can be calculated by eqn (1).

$$\tau_{ave} = \frac{\int_0^{\infty} I(t)tdt}{\int_0^{\infty} I(t)dt} \quad (1)$$

in which I(t) represents the luminescence intensity at a time t.

3. The calculation of $LiTaO_3$:xPr^{3+}(x = 0.000, 0.001, 0.005, 0.025) phosphors energy gap

According to the following equation eqn (2) and (3), the bandgap of the $LiTaO_3$:xPr^{3+}(x = 0.000, 0.001, 0.005, 0.025) phosphors can be estimated:

$$\left[F(R_\infty)h\nu\right]^n = A(h\nu - E_g) \quad (2)$$

where $F(R_\infty)$ represents the Kubelka-Munk function, n equals 2 as the $LiTaO_3$ host absorption is a direct allowed transition. A represents the proportionality constant, hν stands for the energy per photon. The Kubelka-Munk function $F(R_\infty)$ can be expressed as eqn (2):

$$F(R_\infty) = \frac{(1-R)^2}{2R} = K/S \quad (3)$$

where R denotes the reflection coefficient, K represents the absorption coefficient, and S stands for the scattering parameter.

Table S1. Results of the structural refinement of $LiTaO_3$:xPr^{3+} (x = 0.000, 0.001, 0.005, and 0.025).

Parameter	x = 0.000	x = 0.001	x = 0.005	x = 0.025
Space group	R3c (161)	R3c (161)	R3c (161)	R3c (161)
a (Å)	5.15056(9)	5.15567(13)	5.15590(7)	5.15596(11)
b (Å)	5.15056(9)	5.15567(13)	5.15590(7)	5.15596(11)
c (Å)	13.76476(18)	13.75947(29)	13.77239(15)	13.76908(23)
α=β (deg)	90.0	90.0	90.0	90.0
γ (deg)	120.0	120.0	120.0	120.0
V ($Å^3$)	316.234(16)	316.739(8)	317.066(5)	316.996(7)
Units, z	6	6	6	6
R_p (%)	5.02	4.98	4.90	5.61
R_{wp} (%)	7.65	7.04	6.97	8.27
χ^2	3.40	3.12	3.12	3.27

Table S2. Fractional atomic coordinates and isotropic displacement parameters (Å^2) of $LiTaO_3$:xPr^{3+} (x = 0.000, 0.001, 0.005, and 0.025).

Atom	x	y	z	U_{iso}	Occ
			x = 0.000		
Ta	0	0	0.00150	0.01644	1.000
O	0.04902	0.34371	0.06962	0.01383	1.000
Li	0	0	0.27968	0.01000	1.000
			x = 0.001		
Ta	0	0	0.00120	0.00354	1.000
O	0.04948	0.34785	0.07100	0.00584	1.000
Li	0	0	0.27793	0.01693	0.999
Pr	0	0	0.27793	0.01000	0.001
			x = 0.005		
Ta	0	0	0.00124	0.00354	1.000
O	0.04951	0.34623	0.06939	0.00584	1.000
Li	0	0	0.27724	0.01693	0.995
Pr	0	0	0.27724	0.01000	0.005
			x = 0.025		
Ta	0	0	0.00094	0.00354	1.000
O	0.04941	0.34529	0.06887	0.00584	1.000
Li	0	0	0.27585	0.01693	0.975
Pr	0	0	0.27585	0.01000	0.025

Table S3. The bond length (Å) between atoms of refined samples $LiTaO_3$:xPr^{3+} (x = 0.000, 0.001, 0.005, and 0.025).

Bond length (Å)	x = 0.000	x = 0.001	x = 0.005	x = 0.025
(Li/Pr)-Ta	3.0533	3.0721	3.0797	3.0836
(Li/Pr)-Ta	3.0691	3.0768	3.0850	3.0993
(Li/Pr)-Ta	3.3465	3.3397	3.3359	3.3291
(Li/Pr)-(Li/Pr)	3.7558	3.7576	3.7590	3.7587
(Li/Pr)-O	2.0329	2.0150	2.0227	2.0210
(Li/Pr)-O	2.3140	2.3373	2.3324	2.3430
Ta-O	1.9052	1.9355	1.9176	1.9120
Ta-O	2.0774	2.0529	2.0723	2.0764

Figure S1

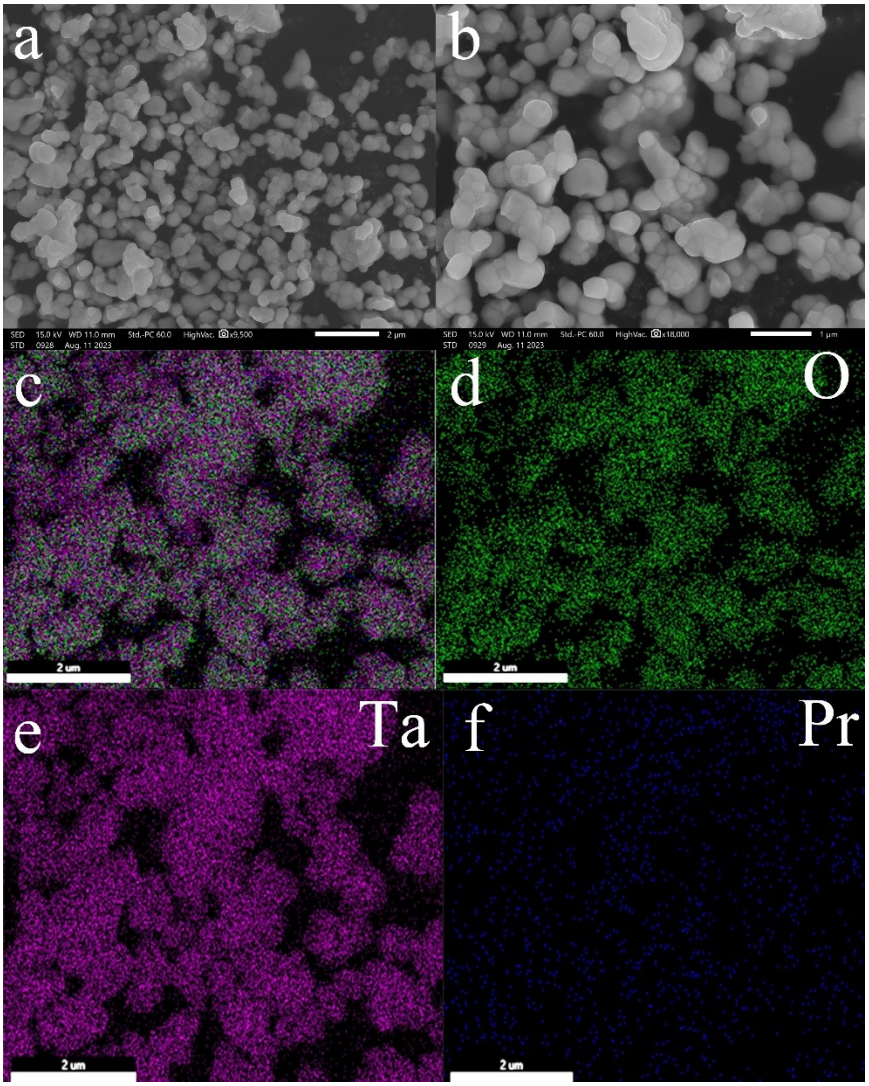

Fig. S1. SEM and mapping analysis for the O, Ta, and Pr elements in $LiTaO_3$:0.001Pr^{3+}.

Figure S2

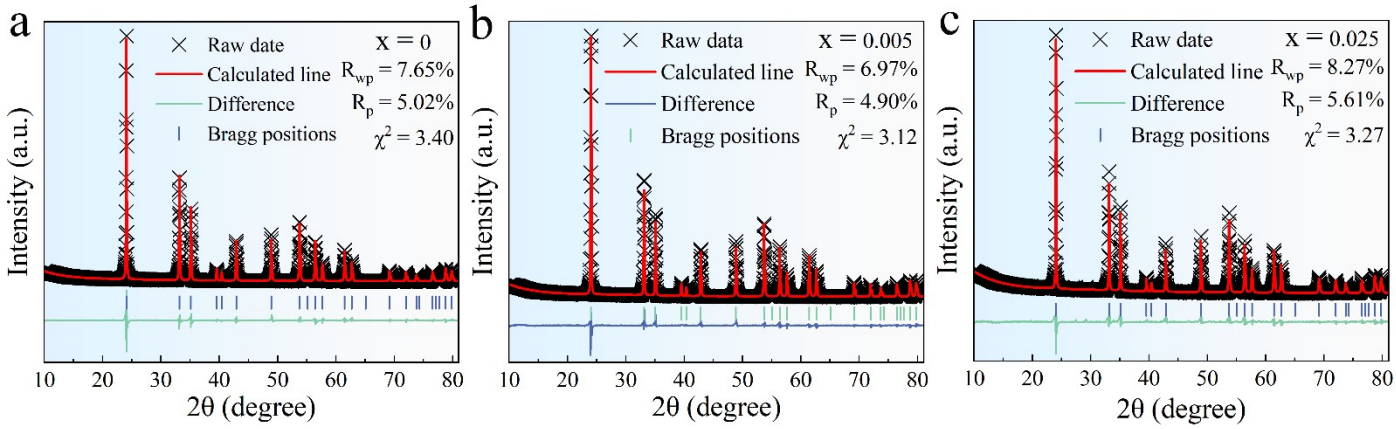

Fig. S2. (a-c) Rietveld refinement patterns for X-ray diffraction patterns of $LiTaO_3$:xPr^{3+} (x = 0.000, 0.005, 0.025).

Figure S3

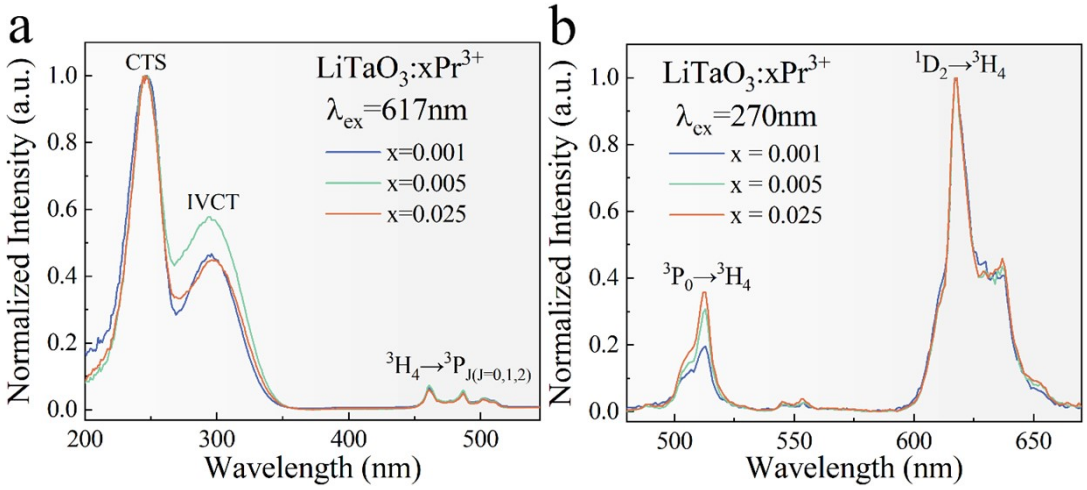

Fig. S3. (a,b) The normalized PLE and PL spectra of $LiTaO_3:xPr^{3+}$ (x = 0.001, 0.005, 0.025).

Figure S4

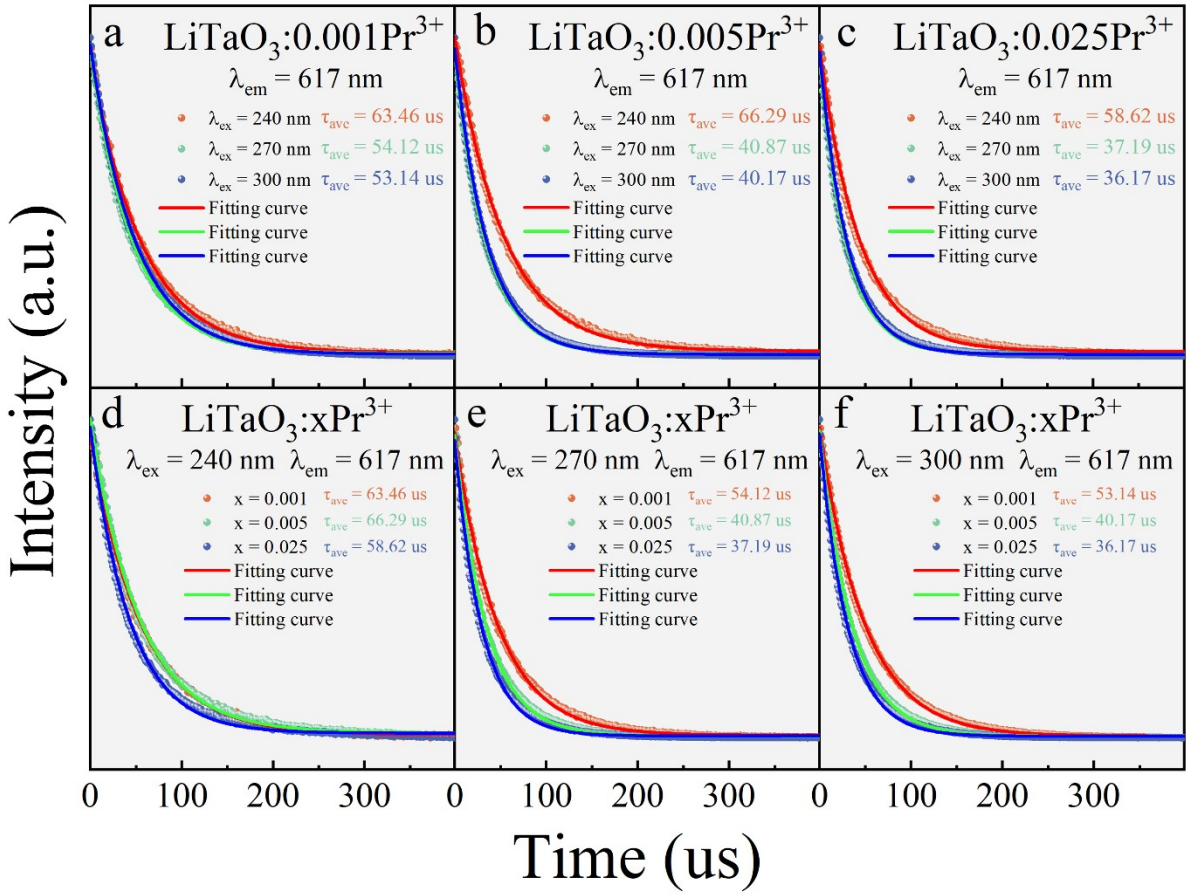

Fig. S4. Fluorescence decay curves of Pr^{3+} $^1D_2$-$^3H_4$ transition under 240, 270, and 300 nm excitation for $LiTaO_3:0.001Pr^{3+}$ (a), $LiTaO_3:0.005Pr^{3+}$ (b), and $LiTaO_3:0.025Pr^{3+}$ phosphors. Fluorescence decay curves of Pr^{3+} $^1D_2$-$^3H_4$ transition under 240 (d), 270 (e), and 300 nm (f) excitation for $LiTaO_3:xPr^{3+}$(x = 0.001, 0.005, and 0.025) phosphors. The scattered points are the experimental data and solid lines are the fitted curves.

Figure S5

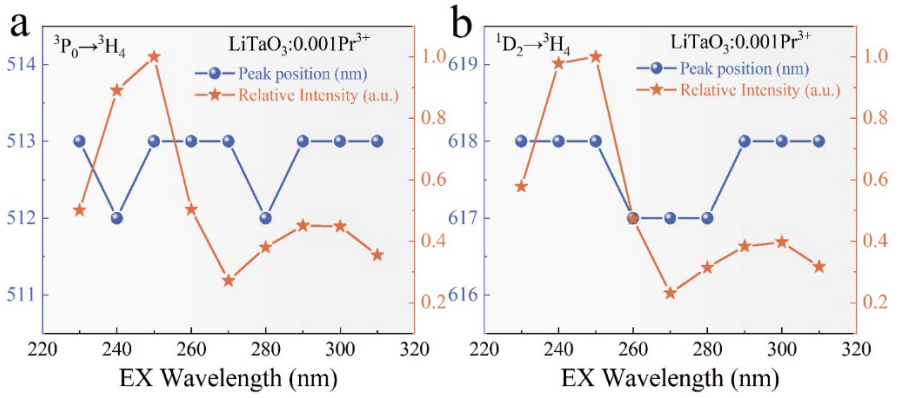

Fig. S5. (a,b) The relationship between $^3P_0 \rightarrow {}^3H_4$, $^1D_2 \rightarrow {}^3H_4$ luminescent properties (peak position and relative intensity) and excitation wavelength in $LiTaO_3$:0.001Pr^{3+}.

Figure S6

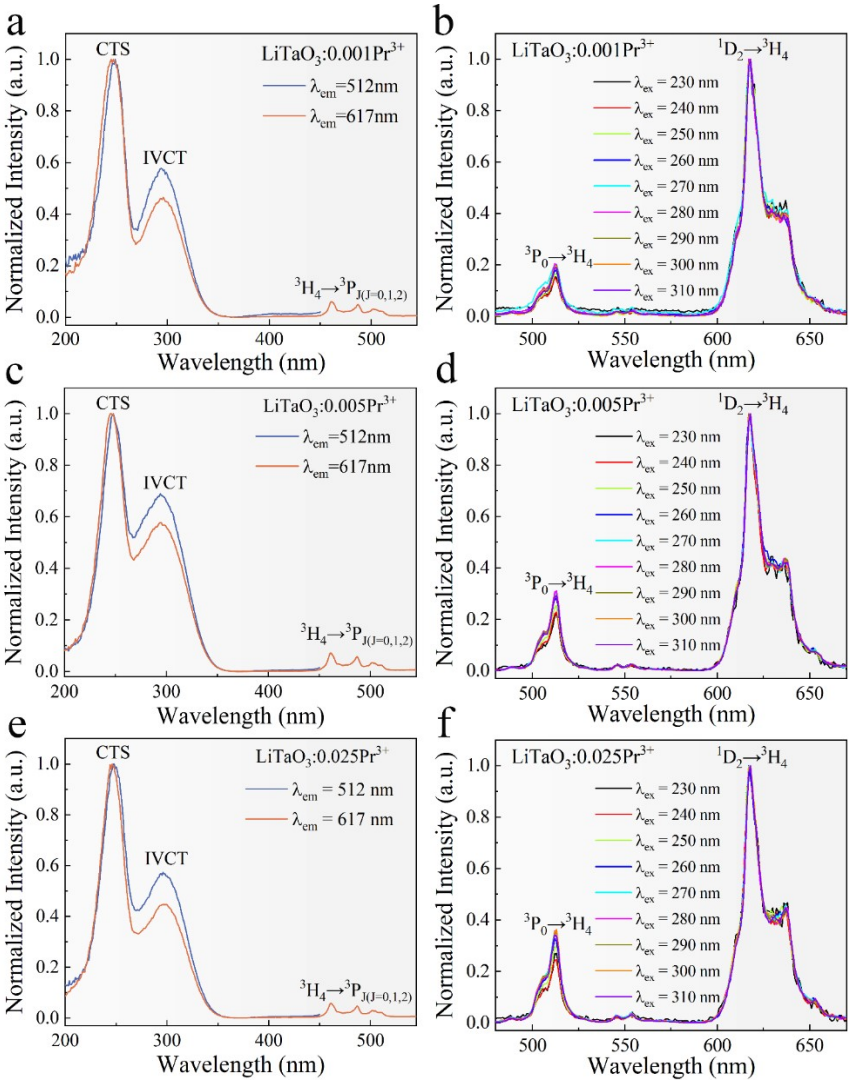

Fig. S6. (a-f) The PLE (at 512 and 617 nm) and PL (at 230-310 nm) spectra of $LiTaO_3$:xPr^{3+} (x = 0.001, 0.005, 0.025).

Figure S7

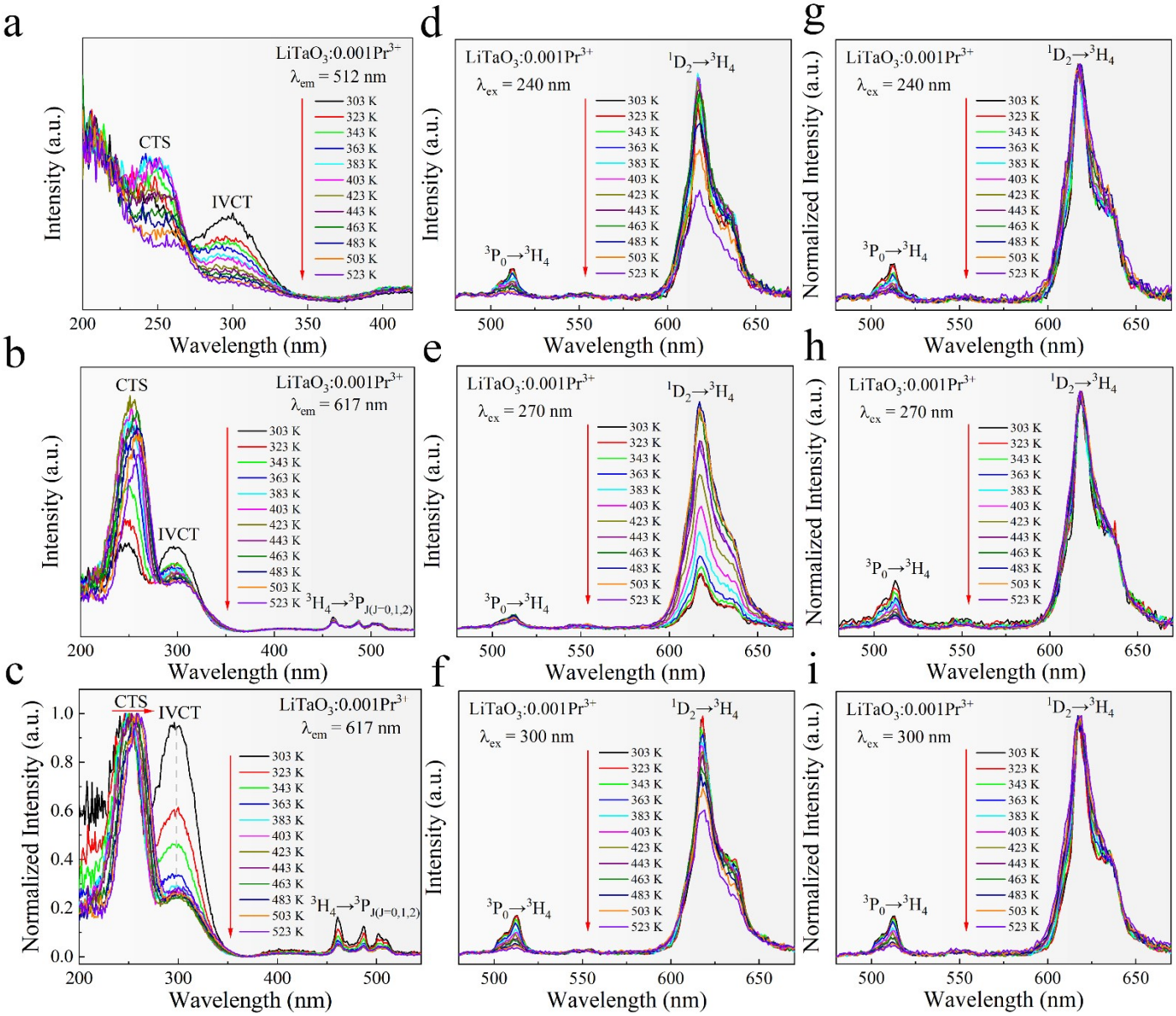

Fig. S7. (a,b) Temperature-dependent PLE (at 512 and 617 nm) spectra from 303 K to 523 K for $LiTaO_3$:0.001Pr^{3+}. (c) Temperature-dependent normalized PLE (at 617 nm) spectra from 303 K to 523 K for $LiTaO_3$:0.001Pr^{3+}. (d-f) Temperature-dependent PL (at 240, 270, and 300 nm) spectra from 303 K to 523 K for $LiTaO_3$:0.001Pr^{3+}. (g-i) Temperature-dependent normalized PL (at 240, 270, and 300 nm) spectra from 303 K to 523 K for $LiTaO_3$:0.001Pr^{3+}.

Figure S8

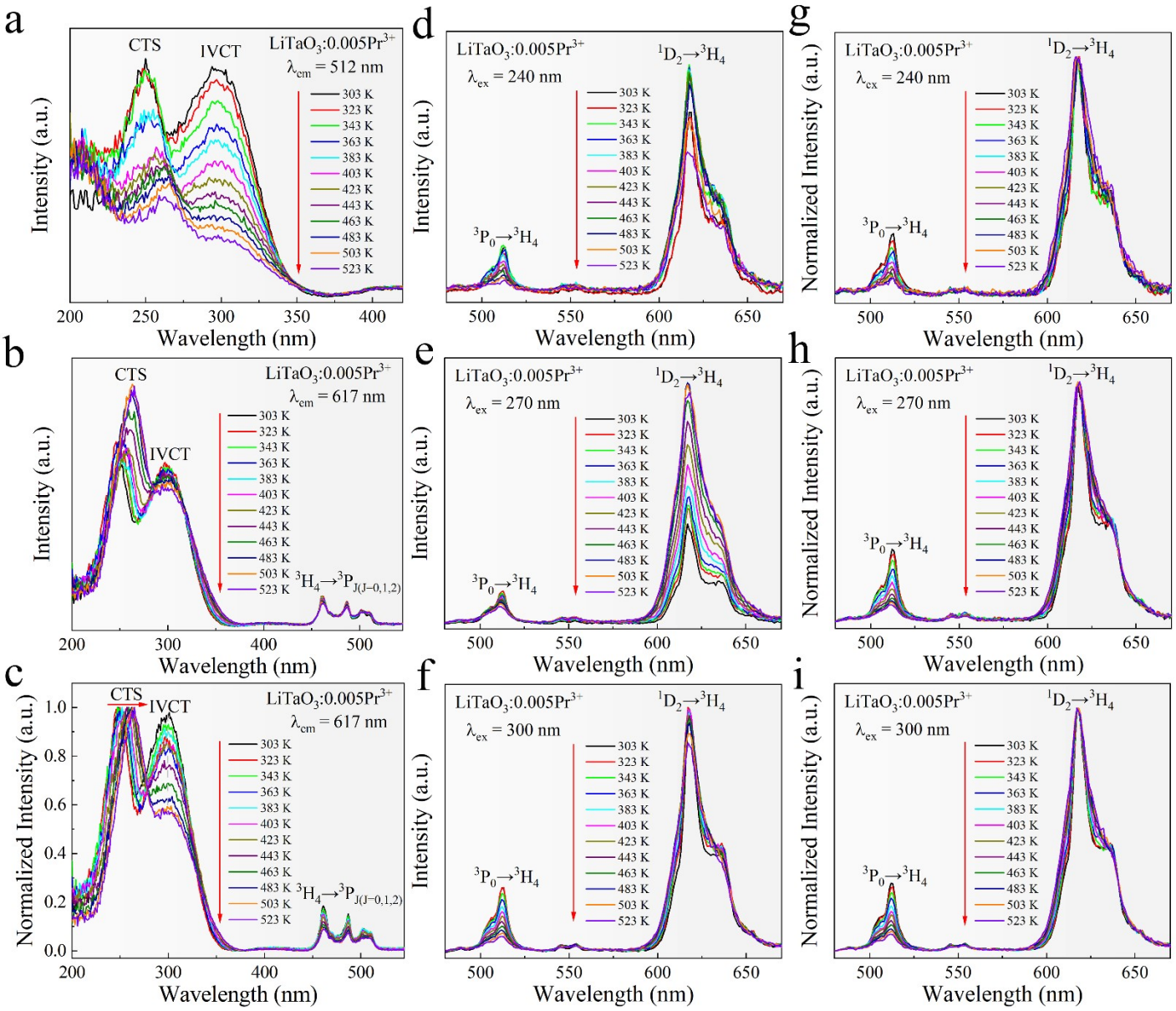

Fig. S8. (a,b) Temperature-dependent PLE (at 512 and 617 nm) spectra from 303 K to 523 K for $LiTaO_3$:0.005Pr^{3+}. (c) Temperature-dependent normalized PLE (at 617 nm) spectra from 303 K to 523 K for $LiTaO_3$:0.005Pr^{3+}. (d-f) Temperature-dependent PL (at 240, 270, and 300 nm) spectra from 303 K to 523 K for $LiTaO_3$:0.005Pr^{3+}. (g-i) Temperature-dependent normalized PL (at 240, 270, and 300 nm) spectra from 303 K to 523 K for $LiTaO_3$:0.005Pr^{3+}.

Figure S9

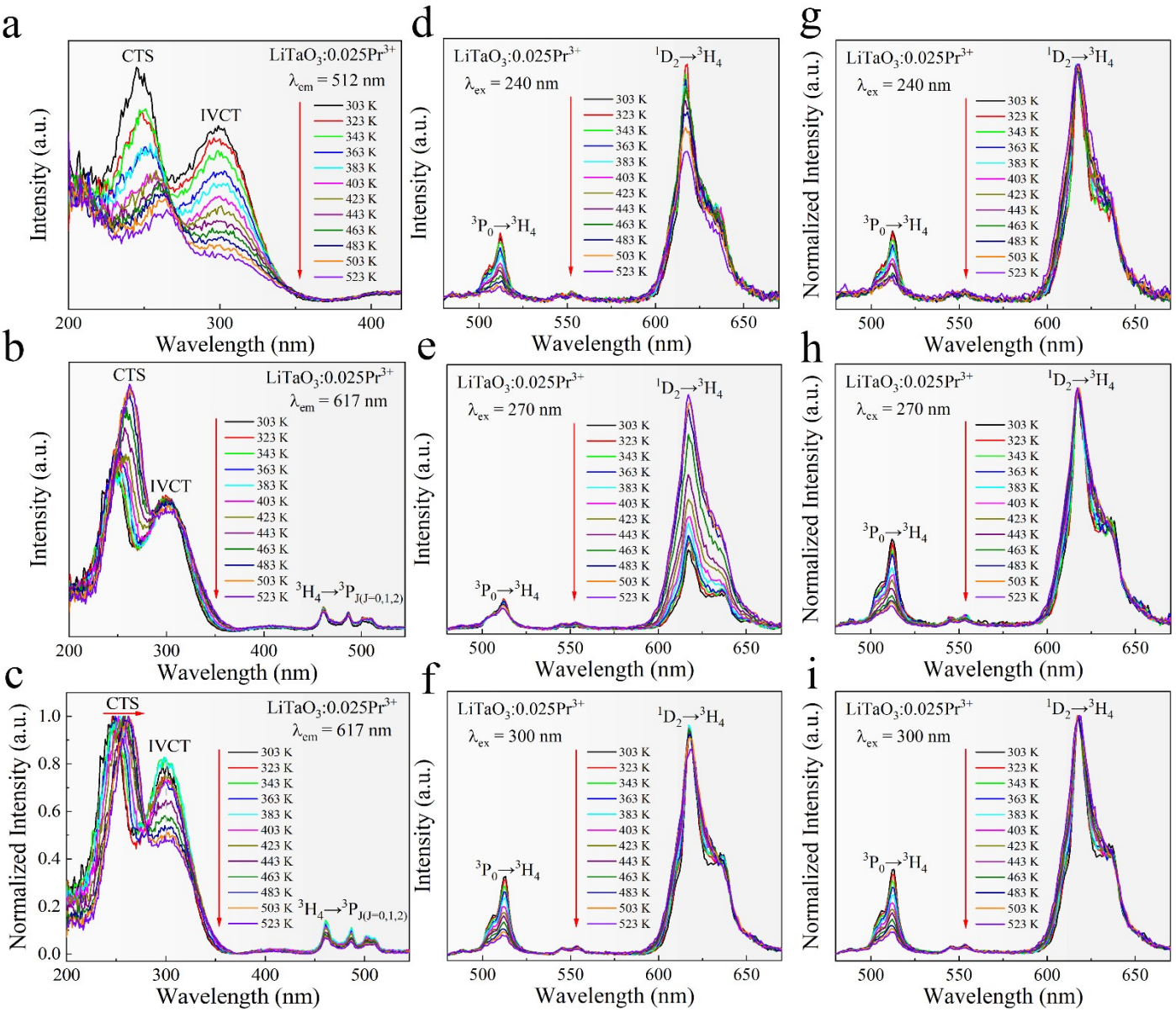

Fig. S9. (a,b) Temperature-dependent PLE (at 512 and 617 nm) spectra from 303 K to 523 K for $LiTaO_3$:0.025Pr^{3+}. (c) Temperature-dependent normalized PLE (at 617 nm) spectra from 303 K to 523 K for $LiTaO_3$:0.025Pr^{3+}. (d-f) Temperature-dependent PL (at 240, 270, and 300 nm) spectra from 303 K to 523 K for $LiTaO_3$:0.025Pr^{3+}. (g-i) Temperature-dependent normalized PL (at 240, 270, and 300 nm) spectra from 303 K to 523 K for $LiTaO_3$:0.025Pr^{3+}.

Figure S10

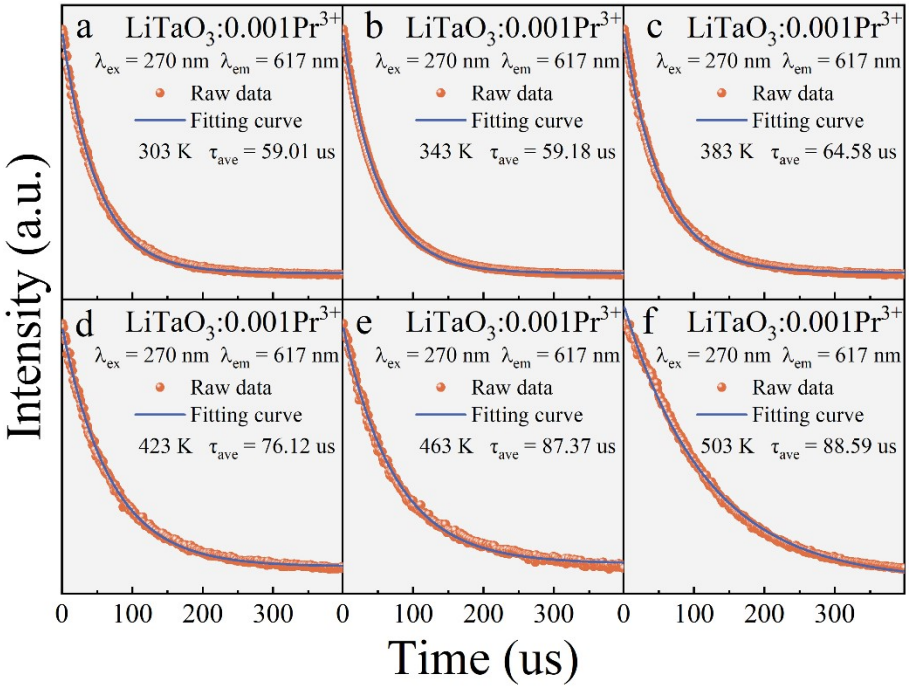

Fig. S10. Fluorescence decay curves of Pr^{3+} $^1D_2$-$^3H_4$ transition under 270 nm excitation from 303 K to 503 K for $LiTaO_3$:0.001Pr^{3+} phosphor.

Figure S11

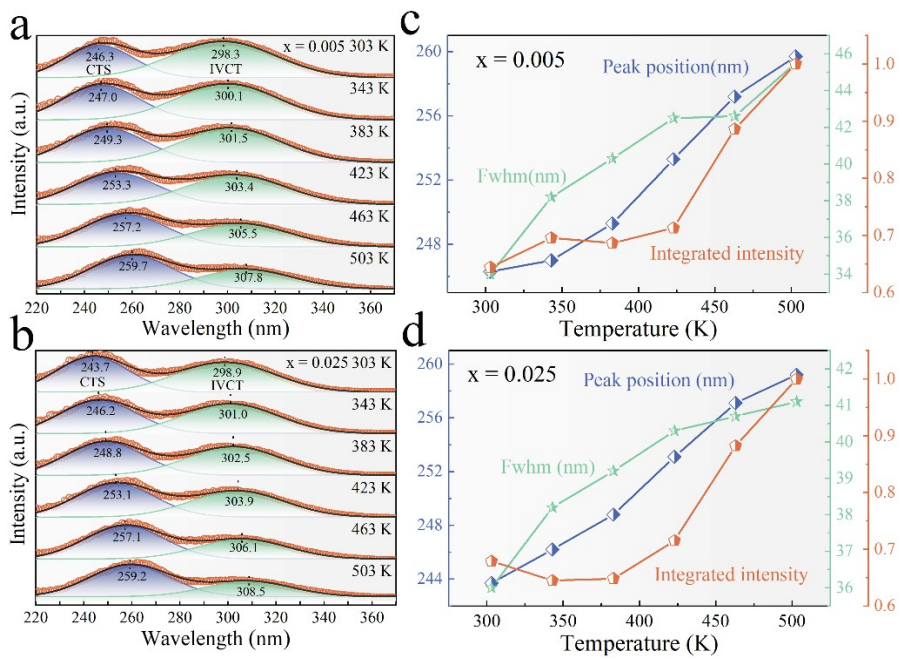

Fig. S11. (a,b) Gaussian fitting of the temperature-dependent PLE spectra of $LiTaO_3$:0.005Pr^{3+} and $LiTaO_3$:0.025Pr^{3+}. (c,d) The relationship between CTS excitation properties (peak position, fwhm, and relative integrated intensity) and temperature in $LiTaO_3$:0.005Pr^{3+} and $LiTaO_3$:0.025Pr^{3+}.

Figure S12

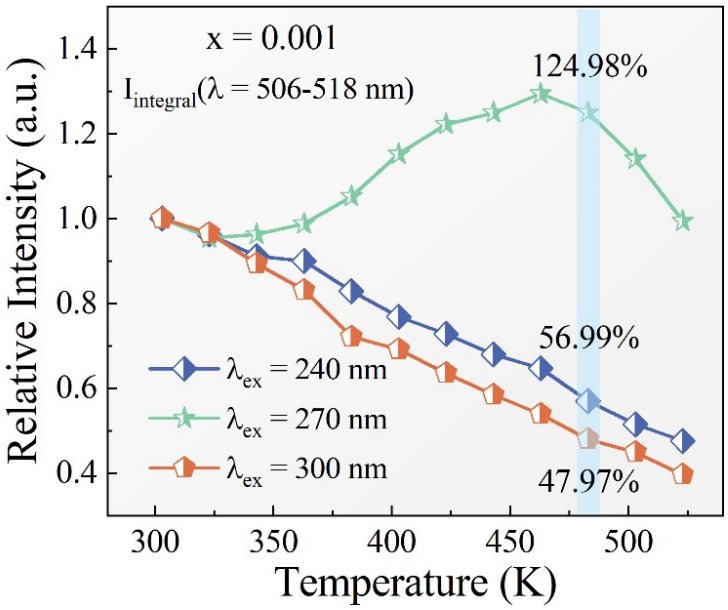

Fig. S12. Relative integral intensity of $^3P_0 \rightarrow {}^3H_4$ PL spectrum at various temperatures under 240, 270 and 300 nm excitation.

Figure S13

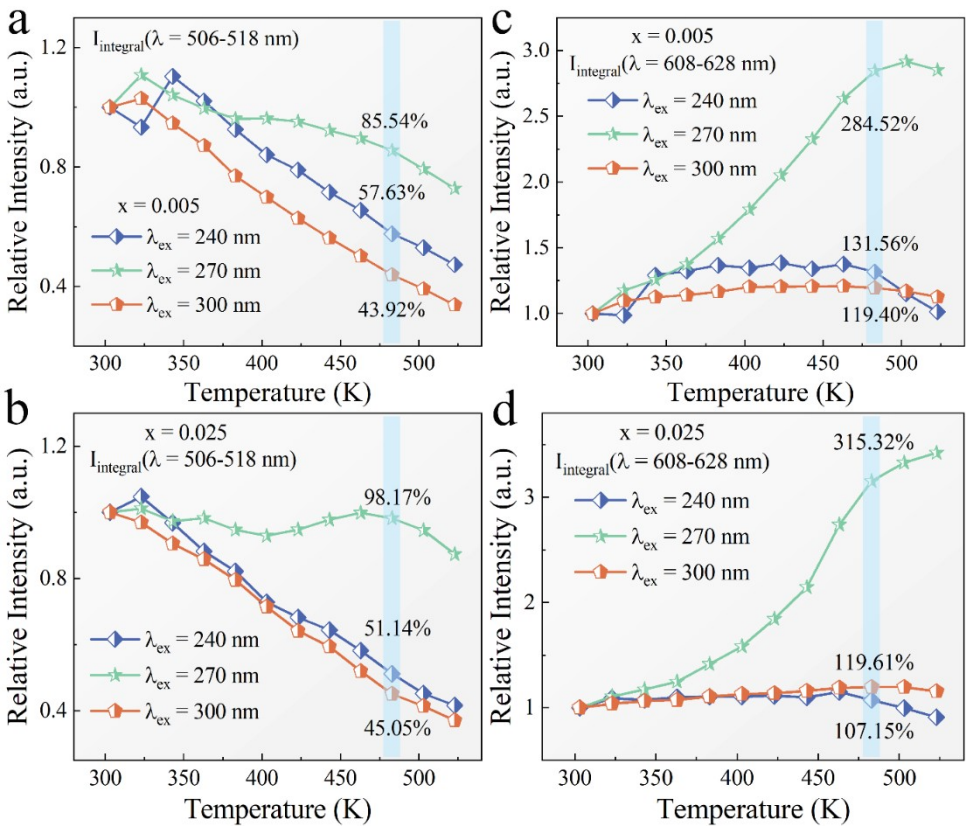

Fig. S13. (a,b) Relative integral intensity of $LiTaO_3$:xPr^{3+} (x = 0.005, and 0.025) $^3P_0 \rightarrow {}^3H_4$ PL spectrum at various temperatures under 240, 270 and 300 nm excitation. (c,d) Relative integral intensity of $LiTaO_3$:xPr^{3+} (x = 0.005, and 0.025) $^1D_2 \rightarrow {}^3H_4$ PL spectrum at various temperatures under 240, 270 and 300 nm excitation.

Figure S14

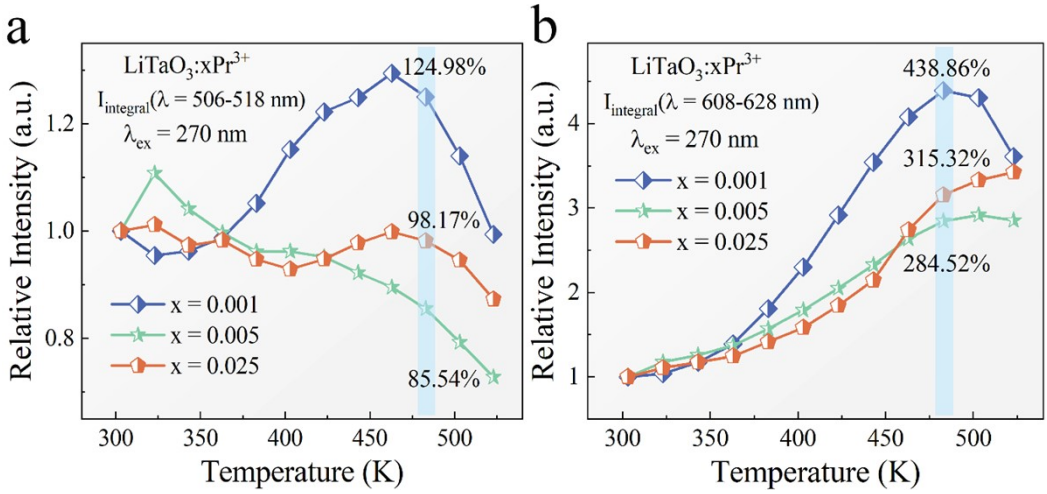

Fig. S14. (a) Relative integral intensity of $LiTaO_3:xPr^{3+}$ (x = 0.001, 0.005, and 0.025) $^3P_0 \rightarrow {}^3H_4$ PL spectrum at various temperatures under 270 nm excitation. (b) Relative integral intensity of $LiTaO_3:xPr^{3+}$ (x = 0.005, and 0.025) $^1D_2 \rightarrow {}^3H_4$ PL spectrum at various temperatures under 270 nm excitation.